Nonisothermal Crystallization Kinetics of Polyamide 6 and Ethylene-*co*-Butyl Acrylate Blends

G. Prasath Balamurugan, S. N. Maiti

Centre for Polymer Science and Engineering, Indian Institute of Technology Delhi, New Delhi 110016, India

Received 4 October 2006; accepted 22 July 2007
DOI 10.1002/app.27377
Published online 9 November 2007 in Wiley InterScience (www.interscience.wiley.com).

ABSTRACT: The nonisothermal melt-crystallization behavior of PA6 and EBA blends at varying EBA content was investigated using differential scanning calorimetry at different scanning rates. Several macrokinetic models such as Avrami, Jeziorny, Ozawa, Liu, Ziabicki, and Tobin were applied to analyze the crystallization behavior thoroughly under nonisothermal conditions. The Avrami and Tobin model predicted that, for pure PA6 and PA6/EBA blends, simultaneous growth of all forms of crystal structures such as fibrillar, disc-like, and spherulitic proceeds at an increasing nucleation rate. However, when applied to blends for isothermal crystallization, the Avrami model predicted that the crystallization process is diffusion-controlled for pure PA6 and PA6/EBA blend containing higher content of EBA (50 phr), where the nylon-6 chains were able to diffuse freely to crystallize under isothermal conditions. Liu model predicted that, at unit crystallization time, a higher cooling rate should be used to obtain a higher degree of crystallinity for both PA6 and PA6/EBA blends. The kinetic crystallizability of PA6 in the blends calculated using Ziabicki's approach varies depending upon the nucleation density and PA6-rich regions present in the blend compositions. Nucleation activity of the blends estimated by Dobreva and Gutzowa method reveals that the EBA particles are inert at lower concentrations of EBA and do not act as nucleating agent for PA6 molecules in the blends. The activation energy of nonisothermal crystallization, calculated using Augis–Bennett, Kissinger, and Takhor methods indicated that the activation energy is slightly lower for the blends when compared to the neat PA6. © 2007 Wiley Periodicals, Inc. J Appl Polym Sci 107: 2414–2435, 2008

Key words: nonisothermal; Avrami; Ozawa; Liu; Ziabicki; Tobin; crystallization kinetics

INTRODUCTION

Polymer crystallization is a phenomenon which occurs during the phase transformation of a polymeric material from the viscous molten state to the semicrystalline solid state. This phase transformation decides the macroscopic structure of the polymeric material and determines the final physical properties of the product.[1,2] When a molten polymer is cooled from the equilibrium melt temperature to a subsequently lower temperature, polymer chains stack themselves to form two-dimensional lamellar structures. This process involves three important stages: *primary nucleation*, *crystal growth*, and *secondary nucleation*.[3] *Primary nucleation* is the process by which a stable crystalline nucleus is formed in the melt state by *homogeneous* or *heterogeneous nucleation*. In homogeneous nucleation, a stable nucleus is formed due to the intermolecular forces, which stacks the macromolecular chains in a parallel array. When the temperature decreases from the melting point to a lower temperature, the intermolecular forces increase in its magnitude and the polymer molecules move toward the lower energy conformation to form stiffer chain segments, which facilitate the chains to arrange themselves in an ordered fashion and thus stable nuclei.[4] In heterogeneous nucleation, the crystallization is catalyzed by the presence of heterogeneities. Very often nucleation of polymers is heterogeneous and starts on surfaces, cavities, or cracks of insoluble impurities, surface from another polymer which is present in the system, etc.

After the nucleus is formed, crystalline lamellae develop and form three-dimensional superstructures. The most common morphology encountered on solidification from the melt is the spherulite, but other superstructures such as hedrites or dendrites form as well.[5] Crystallization generally does not stop with the growth of the crystals, but a process called *secondary crystallization* takes place, producing an increase of crystallinity and thickness of the already formed lamellar crystals, which is commonly encountered in crystalline polymers.

In a *crystalline homopolymer*, the nucleation phenomenon is greatly affected by the chain symmetry, intermolecular forces, tacticity, and branching in the polymer. The growth of a polymer crystal involves thermal diffusion at lower temperatures and thermal

Correspondence to: S. N. Maiti (maitisn49@yahoo.co.in).

redispersion of chains at the crystal/melt interface at high temperature.[6] A chain segment in a polymer can pass through several other crystals adjacent to each other and some portion of the polymer chain remains in amorphous state in-between the adjacent lamellae, and thus not allowing the polymer to crystallize completely. The whole crystallization process involves a complex phase transformation, thermal diffusion, and orientation of polymer chains.

In a polymer/polymer blend or polymer/elastomer blend, the crystallization behavior will be more complicated depending upon the crystallizable nature of the components and their compatibility in the melt state. Composition, processing conditions, crystallization conditions, viscosity, interfacial tension, nature of dispersion, tendency of phase separation, etc. will greatly influence the overall crystallization behavior of the blend.[7] These factors will increase the complexity in the phase transformation, thermal diffusion and orientation of the polymer chains, which will ultimately alter the rate of nucleation and the spherulitic morphology of the system.

In this present work, we have studied the nonisothermal crystallization kinetics of semicrystalline nylon-6 blended with a thermoplastic elastomer, ethylene butyl acrylate copolymer (EBA), at various compositions using differential scanning calorimetry (DSC). Nylon-6 is often modified by blending with a thermoplastic elastomer to improve its notched impact strength, because the improvement is quite distinctive and has been a subject of intense research for more than three decades.[8–12] Even the first nylon blend grade, commercially produced by DuPont in 1975, Zytel St, was modified by maleic anhydride grafted ethylene propylene terpolymer rubber and still has been modified by newly synthesized elastomers. So it is of special interest to study the nonisothermal crystallization kinetics of PA6/EBA (semicrystalline polymer/elastomer blend). Since the polyamide 6 and EBA phases are immiscible, the noncrystallizable EBA is segregated as dispersed phase and the phase morphology of these blends were published in the previous part of our work.[13] In such phase-separated blends, crystallization occurs in the presence of noncrystallizable segregated domains. So during solidification, the dispersed particles must be rejected and/or occluded by the growing spherulites, which markedly disturbs spherulite growth. The separated domains of EBA will mainly remain as a disturbance for the spherulitic growth fronts and may alter the nucleation rate as well. Although the effect of all these phenomena on crystallization behavior of PA6 cannot be completely understood by studying nonisothermal crystallization kinetics, it provides certain useful information regarding the nature of nucleation, rate, crystallizability in the presence of the second phase, the activation barrier, etc.

Although the crystallization has been a subject of intense research for many decades, the theory of crystallization kinetics has been generally confined to isothermal conditions for the sake of mathematical simplicity at constant temperature. However in industrial scenario and practical processing conditions, the crystallization occurs only under dynamic conditions. Thus it is necessary to extend the crystallization kinetics to the nonisothermal conditions.

EXPERIMENTAL

Materials

PA-6 [Gujlon M28RC, density 1.14 g/mL, melt flow index (MFI) 28 g/10 min at 230°C, and 2.16 kg load] was acquired from Gujarat State Fertilizers and Chemicals (Gujarat, India). Ethylene butyl acrylate (Elvaloy 3427AC, density 0.93 g/mL, butyl acrylate content 27% and MFI of 4 g/10 min at 190°C, and 2.16 kg load) was procured from DuPont Industrial Polymers (Wellington, USA).

Melt blending and preparation of test specimens

PA6 and EBA polymers were first vacuum-dried at 80°C and 60°C, respectively, for 3 h. Blends of PA6 and EBA at varying concentrations of EBA 0–50 phr (the blends containing 0, 5, 10, 20, 35, and 50 phr of EBA are designated as PA, PA-5, PA-10, PA-20, PA-35, and PA-50, respectively) were prepared in a corotating intermeshing twin screw extruder, model JSW J75E IV-P (L/D = 36, D = 30 mm), at a screw speed of 240 rpm and temperature profile ranging from 150 to 240°C from the feed zone to the die zone. The extruded strands were granulated. In order to keep the thermal history similar to that of the blends, the component polymers were also extruded under identical processing conditions. The pellets were vacuum-dried for 12 h at 80°C. The pellets were injection-molded on an L&T Demag (model-PFY 40 LNC 4P) machine at a temperature range of 170–260°C from the feed zone to the nozzle and a screw speed of 90 rpm, while keeping the mold temperature constant at (30±2)°C.

Differential scanning calorimetry

The crystallization kinetics was carried out on a Perkin Elmer Pyris-7 DSC with the temperature calibrated with indium. Very small cut portions from the injection-molded tensile specimen of ≈300 to 500 μm size, weighing 5–6 mg, were used for the study to ensure better heat transfer from the DSC pan to the sample.[14] For the nonisothermal crystallization studies, the samples were heated at a constant

heating rate (5, 10, 20, and 30°C/min) from room temperature to 270°C and held there for 2 min to eliminate the residual crystals and memory effects due to thermal and shear history, and subsequently the melt was cooled to crystallize at the same cooling rate under a nitrogen atmosphere to room temperature.

For the isothermal crystallization studies, the samples were heated at a constant heating rate of 30°C/min from room temperature to 270°C and held there for 2 min to eliminate the residual crystals and memory effects due to thermal and shear history. Subsequently, the melt was cooled at the same rate upto 192°C and kept constant at 192°C (isothermal) for 10 min until the sample completely crystallizes.

Wide angle X-ray diffraction patterns

Wide angle X-ray diffraction patterns were recorded for pure PA6 and PA6/EBA blends using a small rectangular piece ($10 \times 12 \times 2.5$ mm^3) cut from the injection-molded samples, on the Philips X-ray diffraction machine, PANalytical diffractometer. Radial scans of intensity (I) vs. diffraction angle (2θ) were recorded in the range of 10–35° of 2θ using Cu K, radiation. Diffractograms of all the samples were recorded at identical settings of the instrument.

RESULTS AND DISCUSSION

Nonisothermal crystallization kinetics

Traditional investigations for the crystallization kinetics of polymers were often limited to idealized conditions at constant temperature, because of the convenience of the theoretical treatment of the data.[15–17] These studies led to better understanding of the basic feature of polymer crystallization, but did not provide sufficient information for processing. In real situation, production and processing of crystallizable polymers are often carried out under nonisothermal conditions, for example, melt-spinning, injection molding and extrusion. During cooling in injection molding of thermoplastics, crystallization process that takes place is generally nonisothermal, with the cooling rates higher than 200°C/min and also the rate of cooling changes with time. It is quite difficult to reproduce and track such conditions using conventional commercial DSC equipment. Several macrokinetic models were often employed to describe the isothermal crystallization process. Despite the large number of models developed for the isothermal crystallization, only a few exist to explain the crystallization under nonisothermal conditions.

Nonisothermal crystallization behavior of PA6 and PA6/EBA blends

The DSC exotherms of neat PA6 and PA6/EBA blends recorded during cooling cycles at different cooling rates such as 10, 15, 20, 30°C/min were depicted in Figure 1. From the DSC exothermic traces of crystallization, the values of relative crystallinity (X_t) at different cooling rates can be calculated according to the following equation:

$$X_t = \frac{\int_{T_o}^{T} (dH_c/dT)dT}{\int_{T_o}^{T_\infty} (dH_c/dT)dT} = \frac{A_o}{A_\infty} \quad (1)$$

where T_o and T_∞ are the temperatures at which crystallization starts (onset temperature) and ends, A_o and A_∞ are areas under the DSC exotherms from T_o to T and T_o to T_∞, respectively. From the relative crystallinity values obtained at different temperatures for different cooling rates, relative crystallinities (X_t) plotted as a function of temperature (T) for PA6 and PA6/EBA blends are shown in Figure 2. It can be seen that all these curves are of similar sigmoidal shapes, implying that there is a lag effect of cooling rate on crystallization. The horizontal temperature axis in Figure 2 can be transferred into a time scale (Fig. 3) by the equation:

$$t = \frac{T_0 - T}{R} \quad (2)$$

where T is the temperature at crystallization time t, T_0 is the initial temperature of crystallization, and R is the cooling rate. Expressed as such, the results show that the higher the cooling rate, the shorter the time for completion of crystallization in PA6/EBA blends. The half-time of crystallization $t_{1/2}$, which is defined as the time to reach 50% of the relative crystallinity, can calculated directly from Figure 3 at $X_t = 0.5$.

From Figures 1–3, some useful DSC crystallization parameters such as onset (T_o) and peak crystallization temperatures (T_p), undercooling temperature (ΔT_c, defined as $T_m - T_p$, where T_m is the actual peak melting temperature of the nonisothermally crystallized sample), and half crystallization time ($t_{1/2}$), corresponding to each cooling rate for all the samples, were listed in Table I. Both PA6 and PA6/EBA blends show a single sharp exotherm in the temperature range of 174–206°C (Fig. 1). For neat PA6 and all PA6/EBA blends, the crystallization exotherms become wider and shift toward lower temperature range with the increasing cooling rate. The parameters such as T_p, T_o, and $t_{1/2}$ decrease with increasing cooling rate, whereas ΔT_c increases. These phenomena can be explained as follows: a

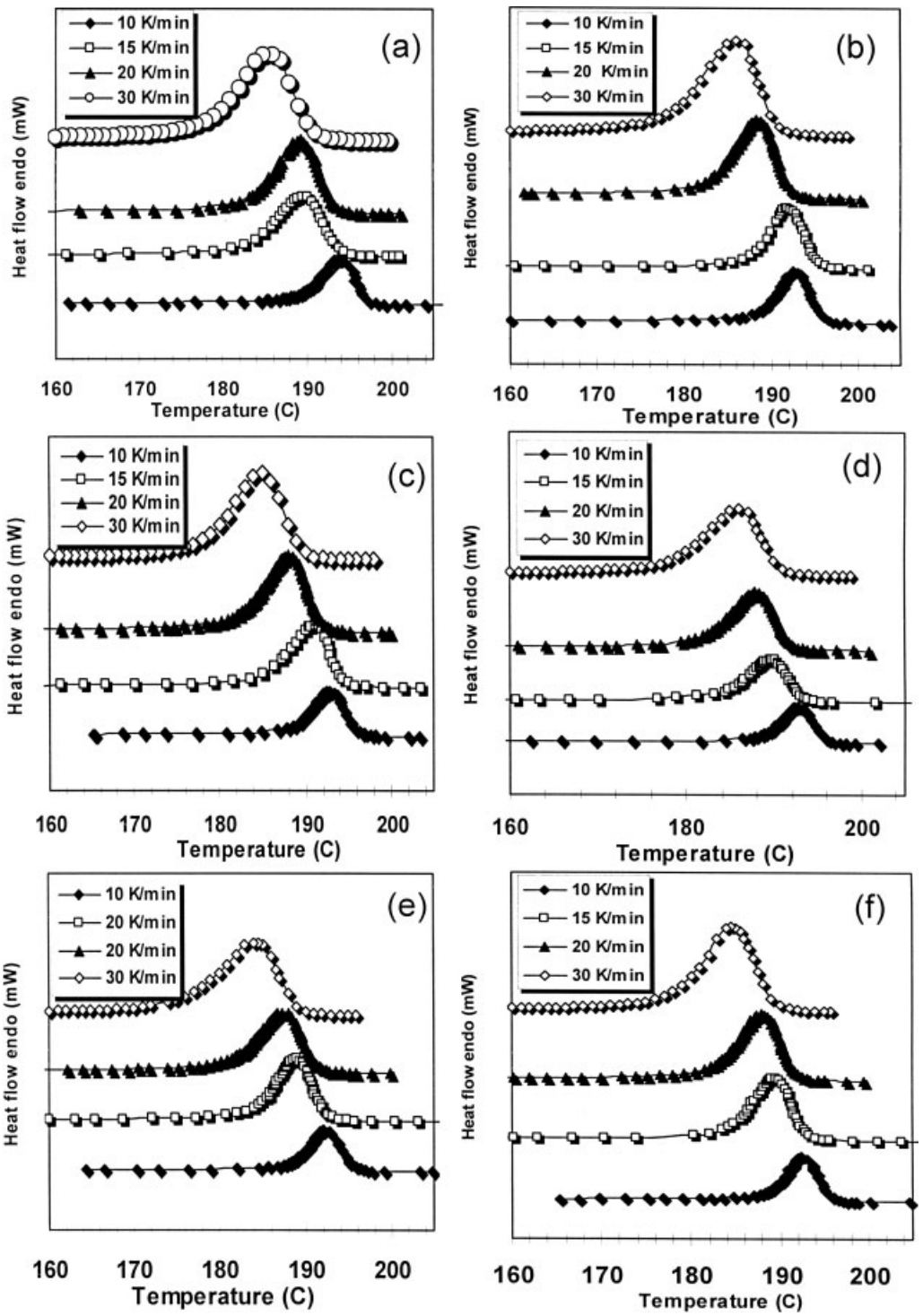

Figure 1 DSC cooling exotherms of PA6/EBA blends at different blend compositions at various cooling rates. (a) PA, (b) PA-5, (c) PA-10, (d) PA-20, (e) PA-35, and (f) PA-50.

higher cooling rate provides a shorter time period for the polymer for its crystallization, whereas the crystallization initiates at a higher undercooling. In addition, the mobility of PA6 molecules cannot follow the cooling rate when the specimens are cooled quickly. However, a marginal decrease in the parameters T_p, T_o, $t_{1/2}$ and slight increase in ΔT_c was observed in all PA6/EBA blends when compared to neat PA6 for the corresponding cooling rates (Table I). These results indicate that the inclusion of EBA elastomeric particles may slightly hinder the motion of the PA6 molecular chains or slightly alter the extent of growth of the PA6 crystals during crystallization.

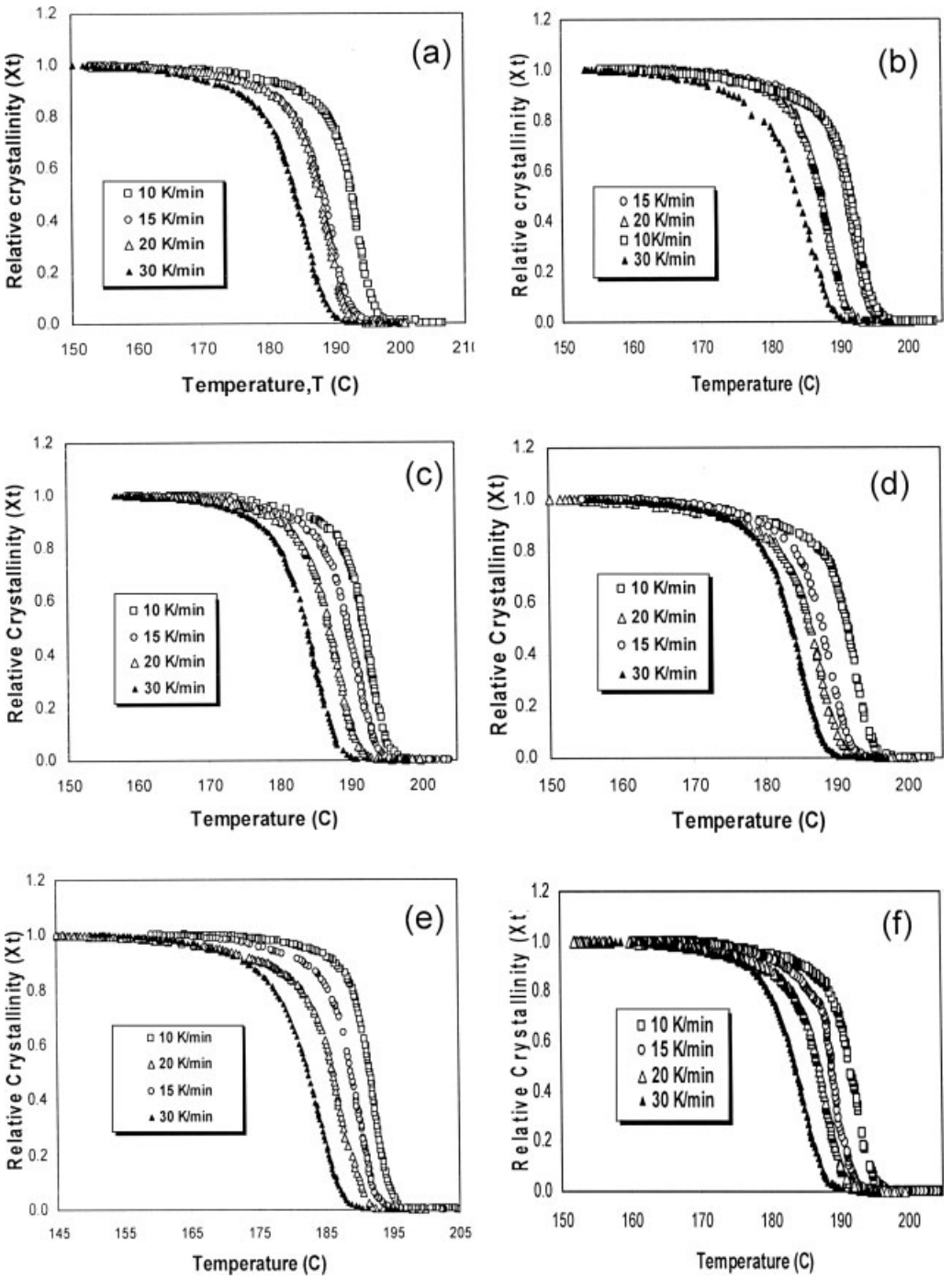

Figure 2 Variation of relative crystallinity versus temperature at various cooling rates during nonisothermal crystallization for (a) PA, (b) PA-5, (c) PA-10, (d) PA-20, (e) PA-35, and (f) PA-50.

Avrami analysis

The overall crystallization kinetics is often interpreted with the aid of the well-known classical Avrami model.[18,19] Although the model describes the crystallization that takes place at constant temperature (isothermal approach), it provides an insight into the process of nucleation and crystal growth that occurs during nonisothermal crystallization. In the isothermal case, assuming that kinetics are controlled by random nucleation and isotropic growth, the fraction of crystallites $X(t)$ transformed between times t and t_0 ($t_0 = 0$) is given by the Avrami equation, Eq. (3):

$$X(t) = 1 - \exp[-k(T)(t - t_0)^n] \quad (3)$$

At constant temperature T, $X(t)$ is the crystalline fraction (dimension less), t is the time (min), k is the crystallization rate constant (min^{-1}), and n is a constant

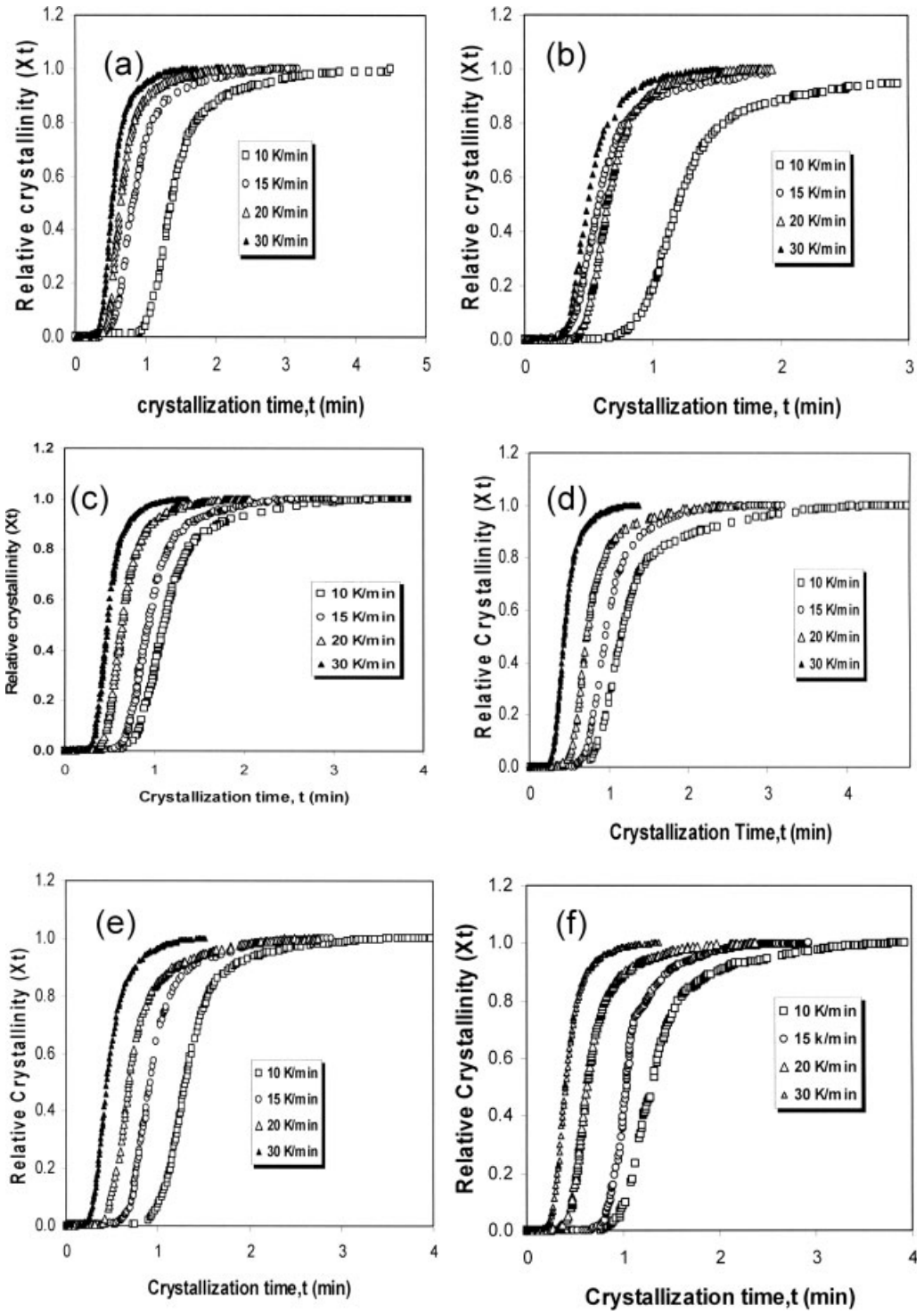

Figure 3 Variation of relative crystallinity versus crystallization time at various cooling rates during nonisothermal crystallization for (a) PA, (b) PA-5, (c) PA-10, (d) PA-20, (e) PA-35, and (f) PA-50.

related to the crystallization mechanism or dimension of growth of the crystallites. In order to simplify the aforementioned equation, it is often expressed in the double logarithmic linear form as given in Eq. (4):

$$\log[-\ln(1 - X_t)] = \log k(T) + n \log t \quad (4)$$

Plotting $\log[-\ln(1 - X_t)]$ against $\log(t)$ for each cooling rate, a straight line could be obtained and from the intercept and slope of the plot, the two adjustable parameters, k and n, can be obtained. Both k and n are the parameters used to qualitatively interpret the crystalline morphology and type of

TABLE I
Crystallization Parameters for PA6 and PA6/EBA Blends Obtained from DSC Cooling Exotherms at Various Cooling Rates

Sample		Designation	R (°C/min)	T_o (°C)	T_p (°C)	ΔH_c (J/g)	ΔT_c (°C)	$t_{1/2}$ (min)
Pristine nylon-6	PA6	PA	10	206.6	193.0	62.87	28.11	1.38
			15	200.9	189.8	64.41	31.35	0.83
			20	200.8	189.0	62.18	31.26	0.65
			30	199.8	185.9	60.44	35.19	0.53
PA6/EBA blends	100/5	PA-5	10	203.8	192.7	62.26	28.51	1.21
			15	199.9	190.3	61.40	30.58	0.59
			20	200.3	187.9	59.63	32.26	0.64
			30	198.0	185.4	48.63	37.36	0.51
	100/10	PA-10	10	203.2	192.5	59.14	28.61	1.11
			15	203.1	189.8	62.53	31.31	0.95
			20	199.8	188.0	62.52	32.23	0.64
			30	198.3	185.4	57.25	37.75	0.48
	100/20	PA-20	10	203.4	192.5	66.83	28.61	1.16
			15	202.6	189.5	60.53	30.21	0.96
			20	200.9	187.6	63.66	32.63	0.73
			30	198.0	184.9	55.03	37.71	0.44
	100/35	PA-35	10	204.7	192.3	66.54	28.79	1.30
			15	202.7	189.8	66.92	31.07	0.92
			20	199.8	187.6	68.87	33.36	0.69
			30	196.0	184.4	62.15	37.32	0.45
	100/50	PA-50	10	204.6	192.3	63.80	28.79	1.31
			15	204.5	189.5	70.44	31.37	1.04
			20	199.5	187.9	63.90	32.39	0.62
			30	195.7	184.9	56.59	39.36	0.41

nucleation for a particular crystallization condition. However, the parameters do not have the same physical significance as in the case of isothermal crystallization, since the temperature changes with respect to time under nonisothermal conditions. This affects the rates of both nuclei formation and spherulite growth, since both the parameters are temperature-dependent. Furthermore, the nonisothermal crystallization rate was characterized by means of half-time of crystallization $t_{1/2}$, which is defined as the time to reach 50% of the relative crystallinity. It can be directly calculated using Eq. (5):

$$t_{1/2} = \left[\frac{\ln 2}{k}\right]^{1/n} \tag{5}$$

From the plot of $\log[-\ln(1 - X_t)]$ against $\log(t)$ (Eq. (4), Fig. 4), it is worth noticing that the nature of the curves changes at different relative crystallinity range. The region where the relative crystallinity $X_t < 0.05$ can be considered as *induction period* where the primary nuclei are formed before the actual crystallites of the nylon-6 macromolecules starts growing. The rate of crystallization in this region is generally very slow and can be neglected for the kinetic studies. The plot of $\log[-\ln(1 - X_t)]$ against $\log(t)$ obey a very good linear fit ($r^2 \geq 0.947$) in the region where the relative crystallinity ranges from $X_t = 0.05$–0.80 (Table II, Fig. 4). This region can be considered as the region of primary crystallization where faster growth of the nylon-6 crystallites occurs after the formation of the primary nuclei. The values of the Avrami exponent n in this region for different cooling rates studied varies in the range of 4.8–6.2 for PA; from 4.3 to 5.6 for PA-5; from 5.3 to 6.1 for PA-10; from 5.1 to 6.0 for PA-20; from 4.2 to 7.3 for PA-35; from 4.6 to 6.6 for PA-50 (Table II). These results suggest that the range of the n values slightly increases as the EBA content increases in the blend. This kind of n values slightly higher than 4 was reported in PA6/Attapulgite composites.[20] According to the predictions of nucleation and growth mechanisms by Avrami (Table III) and later by Christian (Table IV),[21] we can conclude that, since $n > 4$, in this range of $0.05 < X_t < 0.8$ (Fig. 4), there is an increasing rate of nucleation which is no longer constant throughout the transformation process. There may be polymorphic changes from needle-like growth to disc-like or spherulitic growth during the transformation process, which implies that there may be simultaneous appearance of different growth mechanisms during crystallization. Also the density of the growing phase may not be uniform throughout the nylon-6 phase.

The rate of crystallization k value increases from 0.08 to 16.64 min^{-1} for PA and 0.21 to 11.68 min^{-1} for PA-5 as the rate of cooling increases from 10 to 30°C/min (Table II). This implies that the rate of crystallization is higher at higher cooling rate.

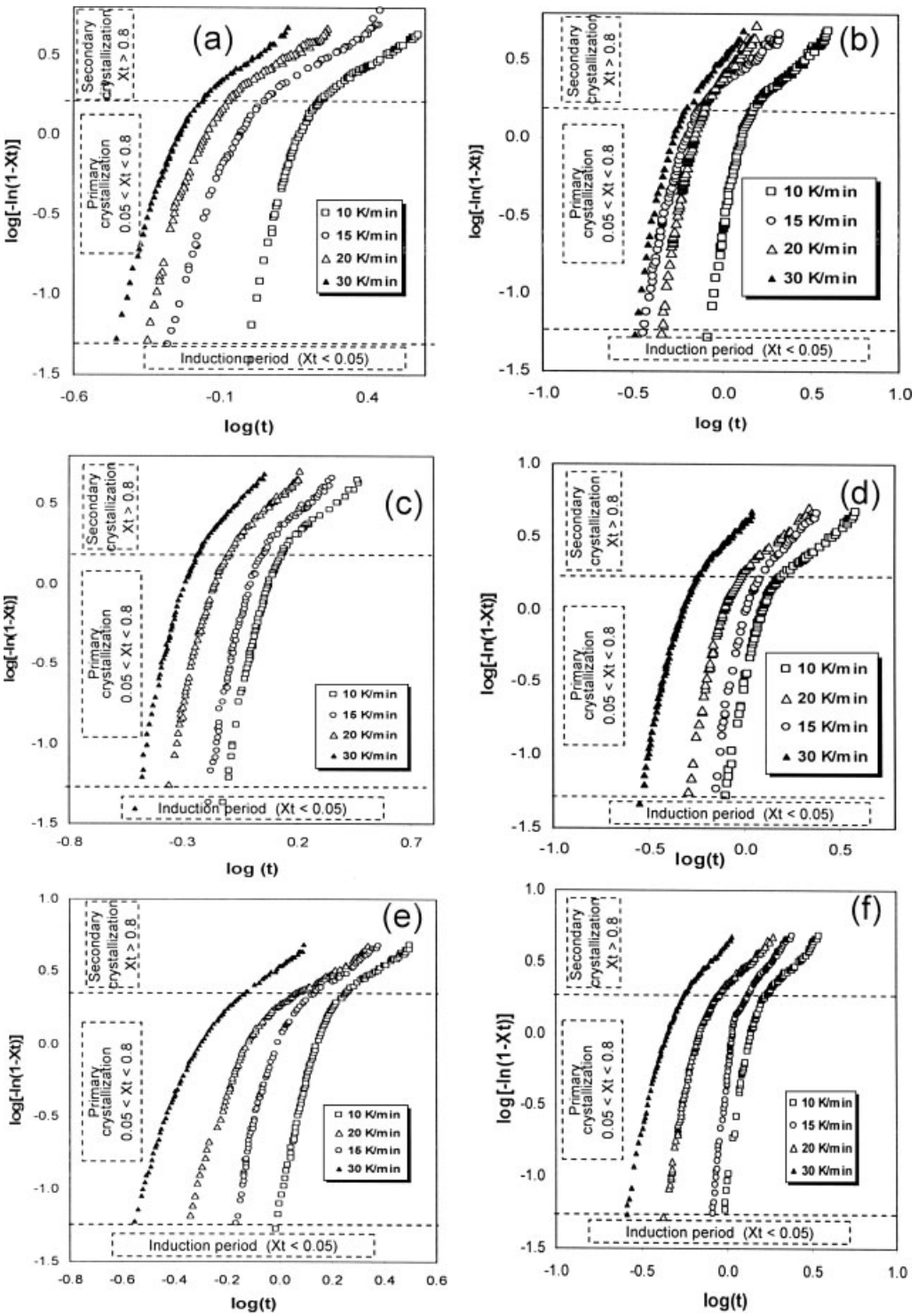

Figure 4 Avrami plots of $\log[-\ln(1 - X_t)]$ versus $\log(t)$ during nonisothermal crystallization for (a) PA, (b) PA-5, (c) PA-10, (d) PA-20, (e) PA-35, and (f) PA-50.

However at higher cooling rate (30°C/min), the k value for PA-5 is much lower than pure PA6 at the same cooling rate (Table II). This suggests that in a two-phase system the dependence of the growth rate on the size of the dispersion is quite strong. The finer the dispersion of the second phase the more is the decrease of spherulitic growth rate.[22] The finer dispersion of EBA in PA6 matrix morphology would have resulted in a stable morphology which strongly affects the crystal growth in PA-5 blend, particularly at higher cooling rate. At higher cooling rates, there is hardly any time for the nylon-6 chains to diffuse

TABLE II
Avrami Parameters During Nonisothermal and Isothermal Crystallization Kinetics for PA6/EBA Blends at Various Blend Compositions

			Nonisothermal kinetics											Isothermal kinetics			
				Primary crystallization			Secondary crystallization			Overall crystallization							
				$5 < X_t$			$80 < X_t < 99$			$5 < X_t < 99$				Temperature = 192°C			
Sample		Designation	R (°C/min)	n	k (min^{-1})	r^2	n	k (min^{-1})	r^2	n	k (min^{-1})	r^2	$t_{1/2}$ (s)	n	K (min$^{-1)}$	$t_{1/2}$ (s)	r^2
Pristine nylon-6	PA6	PA	10	6.2	0.08	0.947	1.2	0.89	0.995	2.5	0.25	0.812	90	2.7	12.20	21	0.998
			15	4.8	1.40	0.970	1.2	1.46	0.980	2.2	0.74	0.877	58				
			20	5.3	5.75	0.950	1.2	2.16	0.991	2.4	1.51	0.864	44				
			30	5.2	16.64	0.971	1.4	2.94	0.994	2.8	3.26	0.881	35				
PA6/EBA blends	100/5	PA-5	10	5.3	0.21	0.961	1.1	1.01	0.987	2.1	0.36	0.851	82	2.6	10.85	21	0.984
			15	4.3	6.02	0.970	1.0	2.12	0.984	2.0	1.46	0.880	41				
			20	5.6	7.31	0.960	1.5	2.38	0.985	2.9	1.96	0.891	42				
			30	4.5	11.68	0.932	1.4	3.14	0.986	2.7	3.37	0.904	33				
	100/10	PA-10	10	5.7	0.33	0.962	1.2	1.12	0.987	3.0	0.39	0.822	72	2.5	10.58	20	0.997
			15	6.1	0.95	0.963	1.4	1.45	0.978	3.2	0.60	0.880	63				
			20	5.3	6.77	0.972	1.4	2.35	0.989	2.8	1.85	0.895	42				
			30	5.4	34.79	0.972	1.6	3.95	0.994	3.2	5.71	0.896	31				
	100/20	PA-20	10	5.2	0.26	0.953	1.1	1.01	0.995	2.1	0.40	0.794	78	2.7	13.65	20	0.984
			15	6.0	0.70	0.966	1.4	1.31	0.999	2.9	1.89	0.870	42				
			20	5.4	3.33	0.953	1.2	1.86	0.992	2.5	1.27	0.814	47				
			30	5.1	40.32	0.975	1.4	3.94	0.991	2.9	5.40	0.907	29				
	100/35	PA-35	10	7.3	0.09	0.981	1.3	1.00	0.985	3.1	0.23	0.840	86	2.5	9.10	21	0.998
			15	6.4	1.03	0.953	1.4	1.43	0.993	3.0	0.58	0.872	64				
			20	4.6	3.33	0.971	1.1	1.86	0.994	2.1	1.27	0.859	45				
			30	4.2	17.25	0.972	1.4	3.37	0.996	2.6	3.97	0.872	30				
	100/50	PA-50	10	6.6	0.11	0.964	1.3	0.95	0.992	2.5	0.32	0.814	82	2.6	14.96	19	0.999
			15	8.5	0.43	0.946	1.6	1.20	0.993	3.1	0.50	0.823	67				
			20	5.1	6.47	0.963	1.2	2.19	0.994	2.6	1.81	0.855	42				
			30	4.6	40.38	0.975	1.4	4.30	0.993	2.8	6.75	0.903	27				

TABLE III
Exponent *n* of Avrami Equation for Different Nucleation and Growth Mechanisms

n	Nucleation and growth mechanisms
3 + 1 = 4	Spherulitic growth + random nucleation
3 + 0 = 3	Spherulitic growth + instantaneous nucleation
2 + 1 = 3	Disc-like growth + random nucleation
2 + 0 = 2	Disc-like growth + instantaneous nucleation
1 + 1 = 2	Fibril-like growth + random nucleation
1 + 0 = 1	Fibril-like growth + instantaneous nucleation

between the finely dispersed EBA domains, which ultimately resulted in lower value of k. However in the other PA6/EBA blends such as PA-10, PA-20, PA-35, and PA-50, the values of k are much higher (from 0.09 to 40.38 min^{-1}) than pure nylon at higher cooling rates. This suggests that the rate of crystallization is higher at higher cooling rates in the blends containing higher content of EBA. This may be due to the fact that, at higher concentration of EBA, the dispersion of EBA domains are relatively poor and coalescence of EBA domains upon rejection by the growing PA6 spherulites dominates. The larger domains of EBA may be engulfed without further rejection by the growing crystal fronts, although the rejection of the particles is usually finished by occlusion or coalescence followed by occlusion. These effects may partially eliminate the growth rate decrease, which increases the overall crystallization rate in the compositions containing higher content of EBA. Furthermore in the presence of EBA domains, the nylon-6 molecules have to crystallize in the interparticle distances between the EBA particles which are of $\sim$ 0.268–0.862 μm.[13] Since the degree of freedom for the mobility of nylon-6 macromolecules in the presence of EBA domains is much low, the nylon molecules which lie in the interparticle distance will try to crystallize instantaneously because of the hydrogen bonding forces between the chains. This hindrance of the lateral growth of the chains to form bigger spherulites and relative ease of formation of smaller spherulites probably led to the increase in the rate of crystallization in the PA6/EBA blends.

In the region where the relative crystallinity X_t = 0.80–0.99 (Fig. 4, Table II), a period of slow crystallization occurs after the spherulites have impinged on one another, which is generally referred to as secondary crystallization. This is the stage where the nylon molecules will try to crystallize over the already formed crystals, which increases the thickness of the crystallite and enhances the crystallinity to some extent. The Avrami crystallization parameters k and n evaluated by linear fitting the plot of $\log[-\ln(1 - X_t)]$ vs. $\log(t)$ in this region are much lower than that evaluated in the primary crystallization region (Fig. 4, Table II). In this region for PA and PA6/EBA blends, the slope n remains almost constant in the range of 1–1.6 (Table II). The values of the rate of the crystallization k are slightly higher at higher cooling rates for both pure nylon-6 and also PA6/EBA blends. However, the rate of transformation is much lower when compared to the primary crystallization.

It is also worth noticing that the overall n values predicted by drawing a linear fit for Avrami plots of $\log[-\ln(1 - X_t)]$ vs $\log(t)$ in the range of $0.05 < X_t$ 0.99, for nonisothermal crystallization, varies from 2.19 to 3.21, with regression coefficient (r^2) values almost ≥ 0.8. This implies that disc-like and spherulitic growth may be predominant. The regression coefficient values ≥ 0.8 suggest that there may be slight deviation from the model. This may be because the Avrami analysis if applied to nonisothermal crystallization may not take care of the effect of secondary crystallization, which may lead to slight deviation in the crystallization behavior from the prediction. The parameters k and n do not have the same physical significance as in the case of isothermal crystallization, since the temperature changes with respect to time under nonisothermal conditions.

Jeziorny corrections for the rate constant and half-time of crystallization during nonisothermal crystallization

Since the temperature changes with respect to time under nonisothermal conditions, it affects the rates of

TABLE IV
A Summary of the Value of *n* Found Under Various Transformation Conditions After Christian[21]

Transformation conditions	*n*
Polymorphic changes, discontinuous precipitation, eutectoid reactions, interface controlled growth, etc.	
Increasing nucleation rate	>4
Constant nucleation rate	4
Decreasing nucleation rate	3–4
Zero nucleation rate (saturation of point sites)	3
Grain edge nucleation after saturation	2
Grain boundary nucleation after saturation	1
Diffusion-controlled growth	
All shapes growing from small dimensions, increasing nucleation rate	>2½
All shapes growing from small dimensions, constant nucleation rate	2½
All shapes growing from small dimensions, decreasing nucleation rate	1½–2½
All shapes growing from small dimensions, zero nucleation rate	1½
Growth of particles of appreciable initial volume	1–1½
Needles and plates of finite long dimensions, small in comparison with their separation	1
Thickening of long cylinders (needles) (e.g., after complete end impingement)	1
Thickening of very large plates (e.g., after complete edge impingement)	½
Precipitation on dislocations (very early stages)	≈2/3

both nuclei formation and spherulite growth, because both the parameters are temperature-dependent. Jeziorny pointed out that the value of the rate constant, k, should be corrected for the rate of crystallization, which depends on the cooling rate employed.[23] Considering the influence of various cooling rates on the nonisothermal crystallization process, Jeziorny gave the final form of the parameter characterizing the kinetics during nonisothermal crystallization as Eq. (6):

$$\ln(k') = \ln(k)/R \tag{6}$$

where k is the crystallization rate constant and k' is the modified crystallization rate constant with respect to cooling rate R. The half-time of crystallization, $t_{1/2}$, for the nonisothermal crystallization can be calculated after correcting the crystallization rate constant k' [Eq. (7)]:

$$t_{1/2} = \left[\frac{\ln 2}{k'}\right]^{1/n} \tag{7}$$

Table V shows the Jeziorny parameters after eliminating the effect of cooling rate. The values of crystallization rate k' are lower at 10°C/min cooling rate for pure PA6 and also for PA6/EBA blends, whereas from 15°C/min to 30°C/min the values exhibit marginal variations in the overall crystallization range ($0.05 < X_t < 0.99$). Similar trend was also observed in the primary crystallization range ($0.05 < X_t < 0.8$); however, the k' values are slightly higher at higher cooling rates. This indicates that the rate of crystallization k' is no longer constant throughout the transformation process at lower cooling rate (10°C/min); however at higher cooling rate, irrespective of the cooling rate the k', values change inappreciably. Furthermore, the half crystallization time, $t_{1/2}$, for the PA6 and PA6/EBA blends are higher to an extent at lower cooling rate of 10°C/min, whereas it remains almost constant within 2–3 s variation at higher cooling rates. This further conforms that the value of $t_{1/2}$ is also a measure of crystallization rate (i.e., reciprocal of half-time, $t_{1/2}^{-1}$) and its variation has the same significance as that of k'.

Isothermal kinetics using Avrami equation

Isothermal DSC runs were conducted at 192°C for pure PA6 and PA6/EBA blends in order to compare the change in the crystallization behavior with that under the nonisothermal conditions. The DSC exotherms and the corresponding variation of relative crystallinity with time during isothermal run for PA6 and PA6/EBA blends were depicted in Fig. 5(a,b), respectively. The Avrami plots of $\log[-\ln(1 - X_t)]$ against $\log(t)$ [Fig. 5(c)] is very linear with regression coefficient values above 0.99, suggesting that the Avrami equation holds good for isothermal crystallization. The values of n for PA6

TABLE V
Jeziorny Parameters Evaluated for Nonisothermal Crystallization Kinetics of PA6/EBA Blends at Various Blend Compositions

			Primary crystallization	Overall crystallization	
Sample	Designation	R (°C/min)	k' (min^{-1})	k' (min^{-1})	$t_{1/2}$ (s)
Pristine nylon-6	PA	10	0.78	0.87	55
		15	1.02	0.98	51
		20	1.09	1.02	51
		30	1.10	1.04	52
PA6/EBA blends	PA-5	10	0.86	0.90	53
		15	1.13	1.03	49
		20	1.10	1.03	52
		30	1.09	1.04	52
	PA-10	10	0.90	0.91	55
		15	1.00	0.97	54
		20	1.10	1.03	52
		30	1.13	1.06	53
	PA-20	10	0.87	0.91	53
		15	0.98	1.04	52
		20	1.06	1.01	51
		30	1.13	1.06	52
	PA-35	10	0.78	0.86	56
		15	1.00	0.96	54
		20	1.06	1.01	50
		30	1.10	1.05	51
	PA-50	10	0.80	0.89	54
		15	0.95	0.95	54
		20	1.10	1.03	52
		30	1.13	1.07	51

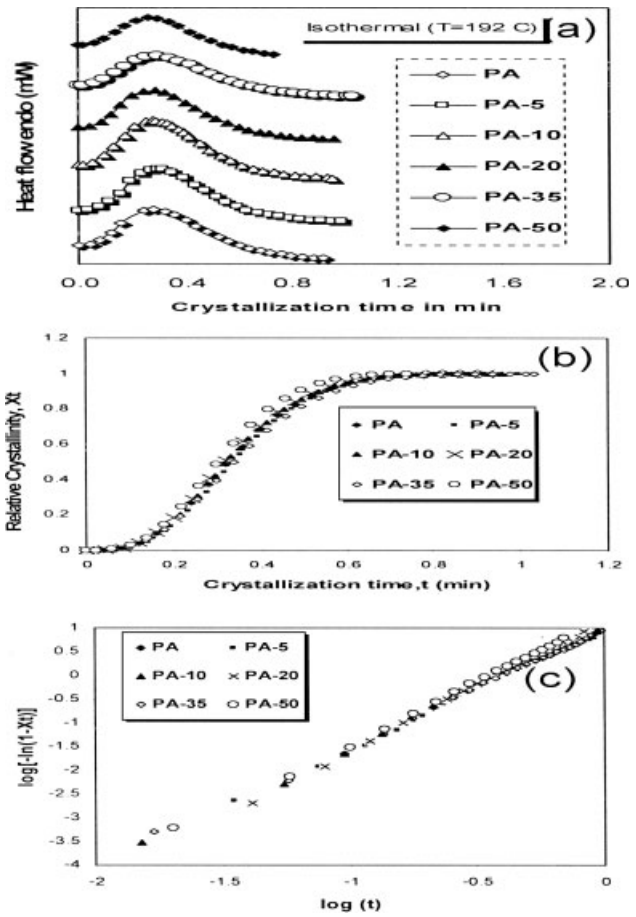

Figure 5 Isothermal crystallization (at $T = 192°C$) parameters variation for PA6/EBA blends at various blend compositions: (a) isothermal crystallization exotherms, (b) relative crystallinity versus crystallization for PA6/EBA blends, (c) Avrami plots of $\log[-\ln(1 - X_t)]$ versus $\log(t)$.

and PA6/EBA blends are almost constant at 2.6, which imply that the nucleation and growth mechanisms are quite similar in the pure component and the blends (Table II). The values of the Avrami exponent n is in the range reported for nylon-6/foliated graphite nanocomposites, under isothermal crystallization conditions.[24] The integer values of n greater than 2.5 suggest that the crystallization is diffusion-controlled with all forms of crystals growing at an increasing nucleation rate during isothermal crystallization. However, the crystallization rate constant k values are higher for pure PA6 and PA-50. This is because for pure PA6, during isothermal crystallization, the crystallization process occurs by homogeneous nucleation. Since the transformation is highly diffusion-controlled, in the absence of EBA domains, the nylon macromolecules can freely diffuse at a higher rate which will favor the faster growth of the crystals. Similarly at higher EBA content (PA-50), there will be nylon-rich regions in the system due to flocculation (grouping of EBA particles in a particular region of the matrix due to coalescence) of EBA particles. So there will be pure nylon-6 rich regions, where the diffusion is much easier and hence faster growth of crystals is possible. However, in compositions such as PA-5, PA-10, PA-20, and PA-35, since the samples are kept at 192°C for long period of time during the isothermal run, the tendency of gross phase separation and the rejection of EBA domains by growing crystal fronts may slightly lower the chain mobility of nylon-6 macromolecules during primary crystallization and may be responsible for slightly lesser values of k. The overall rate of the crystallization can be characterized by the half-time of crystallization ($t_{1/2}$) and the values of $t_{1/2}$ vary from ≈19 to 21 s (Table II) for pure nylon-6 and PA6/EBA blends. This again confirms that the crystallization time required for isothermal crystallization is very less when compared to nonisothermal crystallization, although the initial induction period for the formation of primary nuclei may take a slightly longer duration.

Ozawa analysis

Ozawa extended the isothermal kinetics of crystallization theory to the nonisothermal case on the basis of constant cooling conditions by assuming that the nonisothermal crystallization process comprises of infinitesimally small isothermal crystallization steps or pseudo-isothermal processes.[25] The equation is a modification of the Avrami equation, based on mathematical derivation by Evans,[26] which considers the effect of cooling rate on crystallization from the melt and replaces the crystallization time under isothermal conditions with cooling rate R as follows:

$$1 - X_t = \exp\left[\frac{-K(T)}{R^m}\right] \tag{8}$$

where $K(T)$ is the Ozawa crystallization rate constant, R is the cooling rate, X_t is the relative crystallinity at temperature T, and m is the Ozawa exponent, which is dependent on crystal growth and nucleation mechanism. Ozawa equation can be rearranged into double logarithmic form:

$$\log[-\ln(1 - X_t)] = \log K(T) - m \log R \tag{9}$$

According to the Ozawa analysis, if the relative crystallinities at different cooling rates at a given temperature are chosen, the plot of $\log[-\ln(1 - X_t)]$ vs. $\log R$ should give a series of parallel lines. Then K and m can be determined from the intercept and slope, respectively.

Figures 6 and 7 show the double-logarithmic Ozawa plot of $\log[-\ln(1 - X_t)]$ vs. $\log R$ for all the blend compositions studied, during early stages of

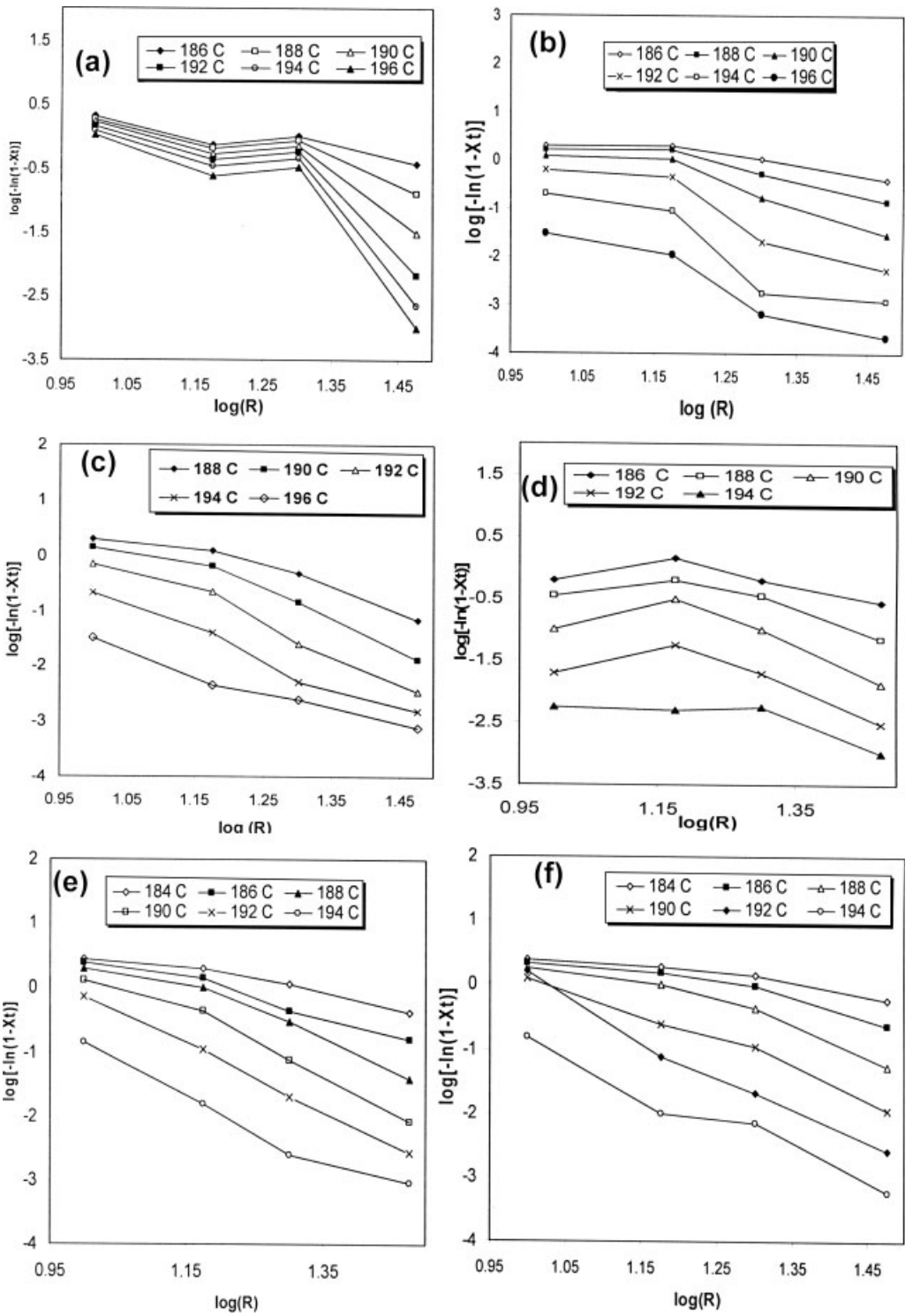

Figure 6 Ozawa plots of $\log[-\ln(1 - X_t)]$ versus $\log(R)$ during early stages (higher temperature range) of nonisothermal crystallization for (a) PA, (b) PA-5, (c) PA-10, (d) PA-20, (e) PA-35, and (f) PA-50.

nonisothermal crystallization (196–184°C) and later stages of nonisothermal crystallization (176°C–166°C), respectively. In both, the stages the behavior are completely different from the predictions by Ozawa model and does not yield any straight line to evaluate the Ozawa exponent m and rate constant $K(T)$. Thus, Ozawa model does not provide a satisfactory description of the nonisothermal crystallization in both the temperature ranges chosen for the study.

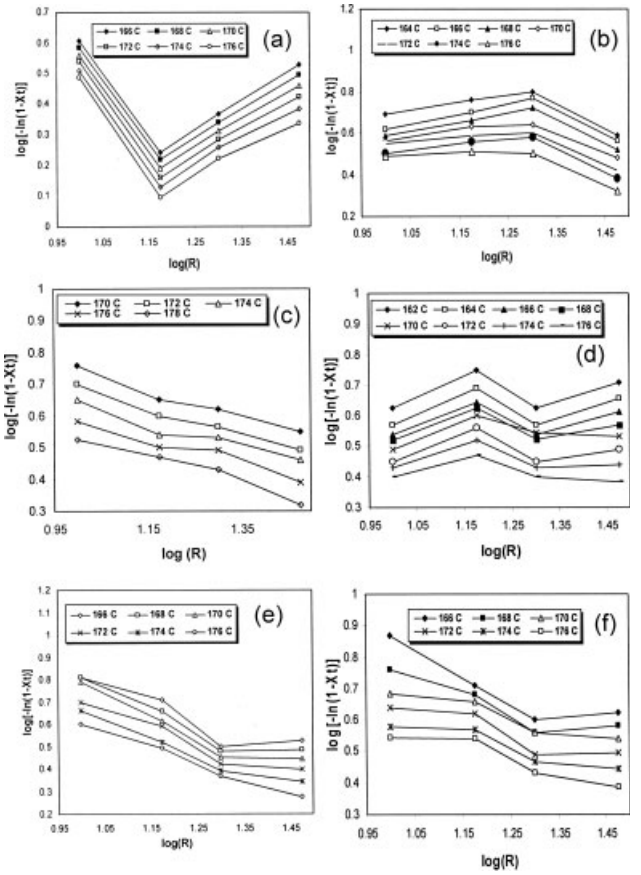

Figure 7 Ozawa plots of $\log[-\ln(1 - X_t)]$ versus $\log(R)$ during later stages (lower temperature range) of nonisothermal crystallization for (a) PA, (b) PA-5, (c) PA-10, (d) PA-20, (e) PA-35, and (f) PA-50.

Liu analysis

Liu developed a new form of kinetic equation by combining Avrami and Ozawa equation for the nonisothermal aspect of crystallization.[27,28] The Avrami equation relates the relative degree of crystallinity X_t with the crystallization time t, and the Ozawa equation relates the relative degree of crystallinity X_t with the rate of cooling R. Thus by combining both the relations [eqs. (4) and (9)] a new kinetic equation for nonisothermal crystallization was derived:

$$\log k + n\ \log t = \log K(T) - m\ \log R \tag{10}$$

which can also be written as

$$\log R = \left[\frac{1}{m}\right]\ \log\left[\frac{K(T)}{k}\right] - \left[\frac{n}{m}\right]\ \log t \tag{11}$$

Rearranging the earlier equation:

$$\log(R) = \log F(T) - a\ \log t \tag{12}$$

where $F(T) = [K(T)/k]^{1/m}$ refers to the cooling rate at the unit crystallization time when the measured system reached a given degree of crystallinity, and a is the ratio of the Avrami exponent (n) to the Ozawa exponent (m). According to Eq. (12), a straight line was obtained by plotting $\log(R)$ against $\log(t)$ (Fig. 8). Values of $F(T)$ and a were calculated from the intercept and slope of plots, respectively, and are listed in Table VI. The plot showed reasonably good agreement for all the compositions studied. However in PA-5 blend, the agreement with the prediction is comparatively less, probably because of the expected phase interaction at lower concentration of EBA, which may alter the course of the crystallization. The smaller the value of $F(T)$, the higher the crystallization rate. Therefore, $F(T)$ had a definite physical and practical meaning. It is evident that the values of $F(T)$ increase with increasing relative degree of crystallinity for PA6 and PA6/EBA blends (Table VI), indicating that at unit crystallization time, a higher cooling rate should be used to obtain a higher degree of crystallinity. The values of a for PA6 and PA6/EBA blends increase slightly with the increase in relative crystallinity, indirectly implying that Ozawa constant m is slightly lesser than Avrami constant n at higher range relative crystallinity, since a is the ratio of n and m. However, the values of a remain closer to unity for PA6 and PA6/EBA blends, suggesting that the nucleation and growth mechanism predicted by Ozawa may be the same for all the compositions as predicted by Avrami.

Ziabicki analysis

Ziabicki introduced a more generalized model to describe the nonisothermal crystallization, which takes into account both transient and athermal effects.[29–31] Ziabicki characterized the kinetics of nonisothermal crystallization by assuming it as a first-order phase transformation process and described it by a simple kinetic equation:

$$dX_t/dt = \lambda(T)[1 - X_t] \tag{13}$$

where X_t is the relative crystallization as a function of time and $\lambda(T)$ is a crystallization rate function which is only dependent on temperature. For a nonisothermal crystallization process, the crystallization rate function, $\lambda(T)$, and relative crystallinity, X_t, vary with temperature and are dependent on the cooling rates studied. Ziabicki showed that the variations in the crystallization rate function, $\lambda(T)$, as a function of temperature can be represented by a Gaussian function of the form:

$$\lambda(T) = \lambda_{\max}\ \exp\left[-4\ \ln 2\,\frac{(T_c - T^2_{\max})}{D^2}\right] \tag{14}$$

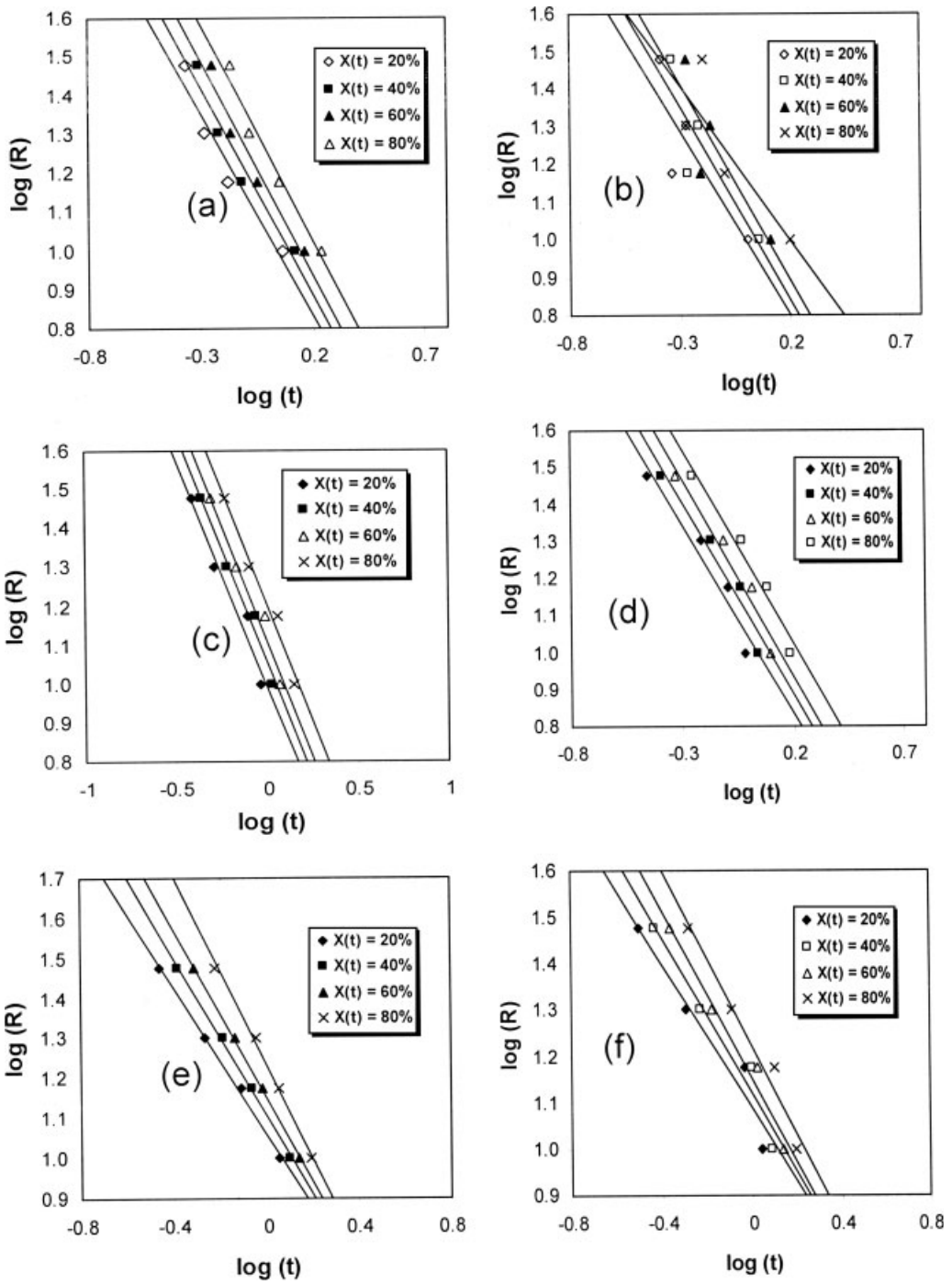

Figure 8 Liu plots of log(t) versus log(R) during nonisothermal crystallization at various relative crystallinity values for (a) PA, (b) PA-5, (c) PA-10, (d) PA-20, (e) PA-35, and (f) PA-50.

where T_{max} is the temperature where the crystallization rate is the maximum; λ_{max} is the crystallization rate corresponding to the temperature T_{max} and D is the half-width of the crystallization rate–temperature function. Assuming isokinetic approximation, integration of Eq. (14) over the whole crystallization temperature range of T_m to T_g leads to an important characteristic value describing the crystallization ability of the polymer, namely, the *kinetic crystallizability G*:

$$G = \int_{T_g}^{T_m} \lambda(T)\, dT \approx 1.064 \lambda_{max} D \qquad (15)$$

The kinetic crystallizability G characterizes the degree of transformation obtained when the polymer

TABLE VI
Liu Parameters for PA6/EBA Blend at Different Blend Compositions at Various Relative Crystallinities

	X_t = 20%			X_t = 40%			X_t = 60%			X_t = 80%		
Sample	a	$F(t)$	r^2	a	$F(t)$	r^2	a	$F(t)$	r^2	a	$F(t)$	r^2
PA	1.05	11.07	0.941	1.08	12.60	0.951	1.12	14.40	0.962	1.13	17.86	0.964
PA-5	0.98	9.92	0.727	1.03	11.05	0.763	1.05	12.60	0.762	0.82	14.62	0.699
PA-10	1.17	9.94	0.962	1.20	11.37	0.973	1.21	13.07	0.969	1.21	16.02	0.969
PA-20	1.03	10.94	0.940	1.05	12.38	0.951	1.07	14.05	0.955	1.06	17.14	0.966
PA-35	0.92	11.54	0.998	0.99	12.80	0.998	1.06	14.20	0.999	1.19	17.19	0.994
PA-50	0.79	12.20	0.944	0.85	13.14	0.953	0.91	14.31	0.973	0.95	16.68	0.971

is cooled at unit cooling rate over the entire crystallization temperature range ($T_g - T_m$). In the case of nonisothermal crystallization studies in DSC where cooling rate is a variable, Eq. (15) can be applied by replacing the crystallization rate function $\lambda(T)$ with a derivative function of the relative crystallinity $X_t^0(T)$ corresponding to each cooling rate studied. Therefore, Eq. (15) can be replaced by

$$G_R = \int_{T_g}^{T_m} X_t^0(T)\, dT \approx 1.064 X^0_{t\,\max,R} D_R \qquad (16)$$

where $X^0_{t\,\max,R}$ and D_R are the maximum crystallization rate and the half-width observed on corresponding derivative function X_t^0 (T). According to Eq. (15), G_R is the kinetic crystallizability at an arbitrary cooling rate R; the kinetic crystallizability at unit cooling rate, G, can therefore be obtained by normalizing G_R with R (i.e., $G = G_R/R$). This procedure was first applied by Jeziorny. Experimental results based on Ziabicki's kinetic crystallizability approach are summarized and the parameters characterizing the nonisothermal crystallization are presented in Table VII. For all the samples (pure PA6 and the blends), the temperature at the maximum crystallization rate $T_{\max}$ is found to decrease with an increasing cooling rate, whereas both the maximum crystallization rate, $X^0_{t\,\max,R}$, and D_R, the half-width of the crystallization rate function X_t^0 (T), were higher at cooling rate R = 30°C/min when compared with the values corresponding to 10°C/min in all the compositions. These results suggest that G_R is an increasing function of the cooling rate. After normalizing the effect of the cooling rate from the resulting G_R values, the values of the kinetic crystallizability at the unit cooling rate G are averaged for all the samples and represented

TABLE VII
Ziabicki Parameters for PA6/EBA Blends Obtained During Nonisothermal Crystallization at Different Blend Compositions at Different Cooling Rates

Sample	R (°C/min)	$T_{\max}$ (°C)	$X^0_{t\,\max,R}$ (10^{-3} s^{-1})	D_R (°C)	D (°C)	D_{avg} (°C)	G_R (°C/s)	G (°C/s)	G_{avg} (°C/s)
PA	10	192.99	5.70	4.71	0.47	0.36	1.71	0.17	0.19
	15	189.77	7.65	6.47	0.43		3.16	0.21	
	20	188.95	10.43	5.60	0.28		3.73	0.19	
	30	185.92	11.49	7.62	0.25		5.58	0.19	
PA-5	10	192.71	5.53	4.76	0.48	0.33	1.68	0.17	0.22
	15	190.28	16.38	4.85	0.32		5.07	0.34	
	20	187.94	9.26	5.63	0.28		3.33	0.17	
	30	185.36	13.48	7.25	0.24		6.24	0.21	
PA-10	10	192.5	6.70	4.39	0.44	0.32	1.88	0.19	0.19
	15	189.78	8.78	5.18	0.35		2.90	0.19	
	20	187.97	11.13	5.71	0.29		4.06	0.20	
	30	185.41	11.99	6.77	0.23		5.19	0.17	
PA-20	10	192.49	6.12	4.30	0.43	0.32	1.68	0.17	0.16
	15	189.46	5.98	5.29	0.35		2.02	0.13	
	20	187.59	9.07	5.71	0.29		3.31	0.17	
	30	184.92	15.43	6.57	0.22		5.19	0.17	
PA-35	10	192.32	5.12	4.28	0.43	0.33	1.40	0.14	0.17
	15	189.79	7.14	5.14	0.34		2.34	0.16	
	20	187.55	8.51	5.71	0.29		3.10	0.16	
	30	184.36	13.35	7.81	0.26		6.60	0.22	
PA-50	10	192.32	11.07	4.25	0.43	0.32	3.00	0.30	0.22
	15	189.5	6.35	5.05	0.34		2.05	0.14	
	20	187.87	10.70	5.54	0.28		3.78	0.19	
	30	184.85	16.64	6.67	0.22		7.08	0.24	

as G_{avg} in Table VII. The physical meaning of the kinetic crystallizability G_{avg} is to characterize the ability of polymers in crystallizing when it is cooled from the melting temperature to the glass transition temperature at a unit cooling rate. The higher the G_{avg} values, the more readily the polymer crystallizes. The crystallization ability of the samples may be arranged in the following order PA-5 $\approx$ PA-50 $>$ PA-10 $\approx$ PA $>$ PA-35 $>$ PA-20. This suggests that the crystallization ability of nylon molecules is slightly higher at lower EBA content (PA-5) due to the fact that smaller size crystallites can be formed without much lateral growth. Similarly, the simultaneous formation of smaller crystallites in the EBA-flocculated regions and larger size crystallites at PA6-rich regions increases the crystallizability at higher EBA content blend, PA-50. Whereas for pure PA6 the crystallizability is purely homogenous, the formation of larger crystallites and lateral growth of the crystallites may be predominant which led to slightly lower value of crystallizability. For PA-35 and PA-20, during crystallization of PA6 molecules, there will be simultaneous movement of the EBA domains inside the matrix because of the tendency of coalescence of the EBA domains due to higher interfacial tension between the PA6 and the EBA.[13] So the mobility of EBA domains may affect the mobility of PA6 molecules which may hinder the crystallizability in these compositions. The half-width of crystallization rate function D_R is higher at higher cooling rates, whereas after normalization with the cooling rate and averaging, D_{avg} is found to be less for PA6/EBA blends compared to PA6. This indicates that the width of the crystallite distribution decreases with the addition of EBA. The WAXD studies also reveal that addition of EBA slightly increased formation of γ-form of crystals and hindered the growth of α-form of crystals, which might be the reason for the reduction in crystallite size distribution (Figs. 12 and 14).

Tobin analysis

Tobin derived a relation between relative crystallinity and crystallization time during the phase transition based on Avrami equation, which is actually a different approximation of Avrami model,[32–34]

$$X_t = \left[\frac{k_t t^{n_t}}{1 + k_t t^{n_t}}\right] \tag{17}$$

where X_t is the relative crystallinity as a function of time; k_t the Tobin crystallization rate constant; and n_t the Tobin exponent. The exponent of time n_t is governed directly by different types of nucleation and various types of growth mechanisms. Equation (17) can be represented in logarithmic form:

$$\ln[X_t/(1 - X_t)] = n_t \ln(t) + \ln(k_t) \tag{18}$$

Based on the variation of relative crystallinity $X(t)$ as a function of time t shown in Figure 3, the Tobin crystallization kinetic parameters (k_t and n_t) can be determined from the intercept and slope of double logarithmic plot of $\ln[X(t)/(1 - X(t))]$ versus $\ln(t)$ [Eq. (17), Fig. 9]. The slope was calculated for 5–99% relative crystallinity, over the entire crystallization range. Values of n_t and k_t for all of the samples are summarized in Table VIII. The value of n_t varies in the range of 4.8–5.5 for PA; 4.0–5.8 for PA-5; 5.4–6.4 for PA-10; 3.8–5.8 for PA-20; 4.0–5.8 for PA-35; 4.7–6.0 for PA-50. These values are closer to the range predicted by Avrami, as significance of the parameter n_t is the same as that of n. Similar to Avrami crystallization rate constant k, the Tobin rate constant k_t shows almost an increasing trend with the cooling rate in most of the composition studied (Table VIII), suggesting that the rate of crystallization increases as the cooling rate increases during nonisothermal crystallization for most of the compositions studied.

Nucleation activity

The nucleation ability of the EBA in PA6/EBA blends was estimated by a method developed by Dobreva and Gutzowa.[35,36] For homogeneous nucleation from the melt, the cooling rate, R, can be written as follows:

$$\log(R) = A - \frac{B}{2.303\Delta T_p^2} \tag{19}$$

where ΔT_p is defined as $T_m - T_p$. T_m and T_p are the peak temperatures of melting and crystallization, respectively, and A and B are constants. For heterogeneous nucleation, the cooling rate is defined as

$$\log(R) = A - \frac{B^*}{2.303\Delta T_p^2} \tag{20}$$

where B^* is a constant. The ratio B^*/B is defined as Φ, the nucleating activity. For a more active substrate the values of Φ is closer to zero; for absolutely inert particles, Φ = 1. Φ is, therefore, the ratio of the slopes of the linear plot of log R as a function of $1/\Delta T_t^2$ for the blend and the pure component (Fig. 10). The values of nucleation activity reported in Table IX. The Φ values are slightly above 1 for PA-5 and PA-10, indicating that EBA does not act as nucleating agent for the matrix nylon at these compositions. However, the Φ values are in the range of 0.6–0.8 for PA-20, PA-35, and PA-50.This indicates that the EBA acts as a nucleating agent, which could be misleading, rather this is due to the fact that addition of EBA has

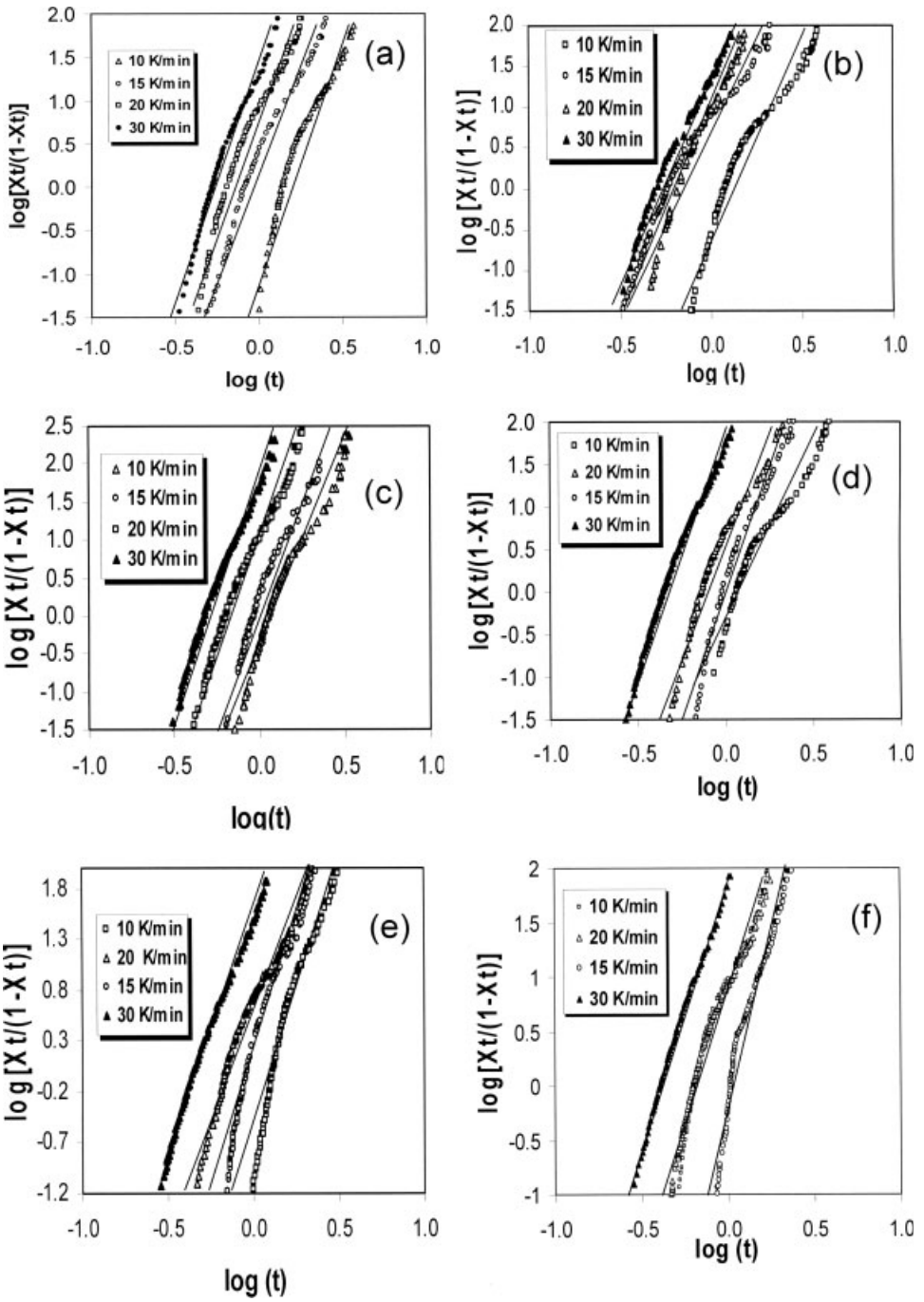

Figure 9 Tobin plots of $\log(t)$ versus $\log[X_t/(1 - X_t)]$ during nonisothermal crystallization at various cooling rates for (a) PA, (b) PA-5, (c) PA-10, (d) PA-20, (e) PA-35, and (f) PA-50.

favored the formation of γ-form of crystals in nylon-6, which is discussed in the later part of the article.

Activation energy of crystallization

The effective activation energy of crystallization ΔE can be determined by methods proposed by Augis and Bennett, Kissinger, or Takhor.[37–39] The primary motive of all these methods is to develop a definite relationship between the peak temperatures T_p obtained from the nonisothermal crystallization exotherms and the cooling rate used. The activation energy values can be calculated based on the plots of the following forms:

Augis Bennet method,

$$\left[\frac{d\left[\ln\left(R/\left(T_0 - T_p\right)\right)\right]}{d\left(1/T_p\right)}\right] = -\frac{\Delta E}{Rg} \tag{21}$$

TABLE VIII
Tobin Parameters for PA6/EBA Blends at Various Cooling Rates at Different Compositions

Sample	R	n_t	k_t	r^2
PA	10	4.8	0.46	0.941
	15	4.5	1.22	0.978
	20	4.7	2.16	0.972
	30	5.5	3.95	0.979
PA-5	10	4.5	0.59	0.956
	15	4.0	2.14	0.975
	20	5.8	2.68	0.981
	30	5.2	4.45	0.979
PA-10	10	5.4	0.69	0.966
	15	5.9	1.07	0.958
	20	5.6	2.60	0.983
	30	6.4	7.02	0.971
PA-20	10	3.8	0.76	0.965
	15	5.8	0.88	0.973
	20	5.2	1.75	0.958
	30	5.4	6.10	0.986
PA-35	10	5.8	0.47	0.968
	15	5.4	1.06	0.974
	20	4.0	1.82	0.975
	30	4.5	4.55	0.994
PA-50	10	4.8	2.37	0.963
	15	6.0	0.85	0.970
	20	4.7	2.38	0.972
	30	5.1	7.01	0.988

Kissinger method,

$$\left[\frac{d\left[\ln\left(R/T_p^2\right)\right]}{d\left(1/T_p\right)}\right] = -\frac{\Delta E}{R^g} \tag{22}$$

Takhor method,

$$\left[\frac{d[\ln R]}{d\left(1/T_p\right)}\right] = -\frac{\Delta E}{R^g} \tag{23}$$

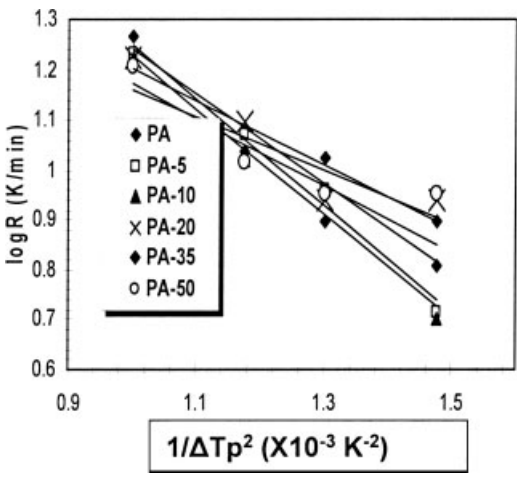

Figure 10 Nucleation activity by Dobreva and Gutzowa approach for various PA6/EBA blend compositions.

TABLE IX
Nucleation Activity Values for Various PA6/EBA Blends at Different Blend Compositions

Sample	Slope (B or B^*)		Nucleation activity (?)
PA	B	895.3	–
PA-5	B^*	1063.6	1.2
PA-10		1049.4	1.2
PA-20		634.4	0.7
PA-35		674.5	0.8
PA-50		529.1	0.6

where T_0 is the initial reference temperature from the melt state (assumed as 240°C), T_p is the crystallization peak maximum, R^g is the universal gas constant (R^g = 8.3145 J/mol/K) and R is the cooling rate.

The activation energies for the samples obtained from the slope of the least-square lines drawn from the plots of Augis and Bennett, Kissinger, and Takhor were listed in Table X and the plots were shown in Figure 11. The absolute values of ΔE are different for different methods. These values are in the range reported in PA6/Attapulgite composites[20] PA6/foliated graphite nanocomposites.[24] Augis–Bennet method was considered to be the most accurate one.[40] However, the variation in activation energy shows a similar trend in all the samples studied irrespective of the method of their evaluation. The activation energy values for the PA6/EBA blends are lower than that of the pure PA6. In general, the activation energy barrier for crystallization in a two-phase immiscible system involves the energy dissipated to perform rejection (related to viscosity of the melt), engulfing or deformation of the noncrystallizable component, kinetic energy required to overcome the inertia of the droplets and energy required for the creation of interfaces.[7] The different thermal conductivity of the amorphous component in the dispersed isles, compared to that of the crystallizable component, also affects crystallization kinetics, as it affects the heat dissipation path.[41] All these complexities should increase the activation energy barrier in the PA6/EBA blends compared to that of the pure

TABLE X
Activation Energy Values for Various PA6/EBA Blends at Different Blend Compositions

	Activation energy, E (kJ/mol)		
Sample	Kissinger	Augis Bennet	Takhor
PA	288.73	245.77	281.02
PA-5	268.72	226.15	261.03
PA-10	283.18	240.65	275.48
PA-20	265.74	223.41	258.04
PA-35	249.91	207.94	242.22
PA-50	270.59	228.40	262.90

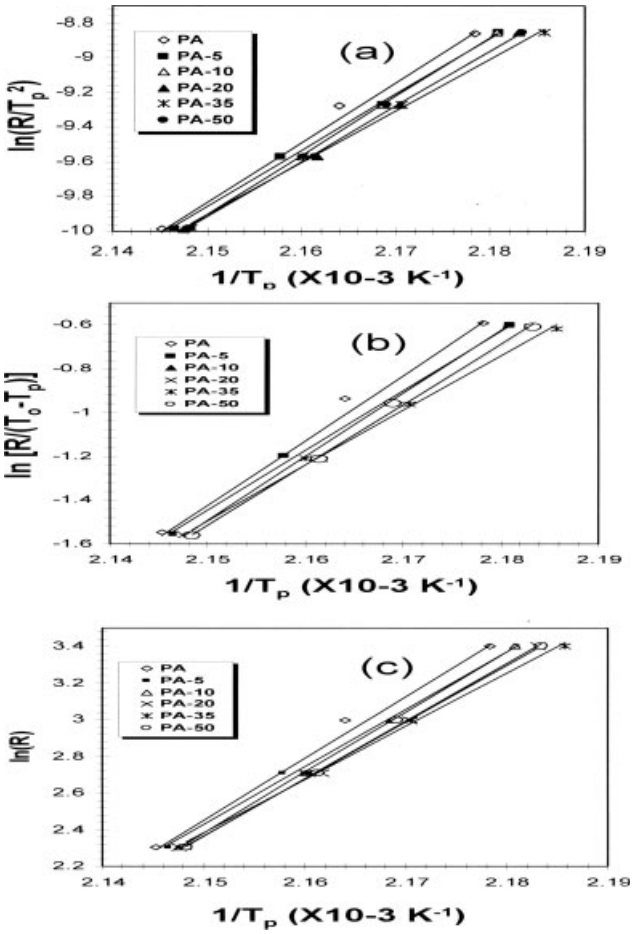

Figure 11 Activation energy of crystallization during nonisothermal crystallization for different blend compositions by (a) Kissinger method, (b) Augis–Bennet method, and (c) Takhor method.

PA6. Rather the decrease in activation energy in the blends may be due to a drastic decrease in the proportion of α-form crystals and a slight increase in the proportion of γ-form of crystals in PA6 upon addition of EBA. The decrease in α-form crystals and increase in γ-form of crystals on addition of EBA were revealed by wide angle X-ray diffraction studies (Fig. 12). The presence of an elastomeric phase in a semicrystalline matrix will induce mechanical restraints to the mobility of PA6 chains. In PA6/EBA blends, the restraints caused by the presence of EBA favor the growth of γ-form and hinder growth of α-form. The decrease in the α-form has led to the decrease in the activation energy of PA6/EBA blends when compared to neat PA6.

Wide angle X-ray diffraction studies

Wide angle X-ray diffraction patterns of PA6 and PA6/EBA blends at varying blend compositions were depicted in Figure 12. It reveals the presence of

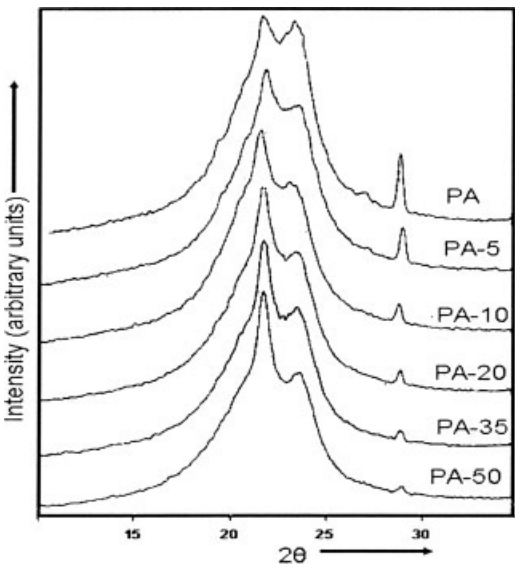

Figure 12 Wide angle X-ray diffraction patterns of PA6/EBA blends at varying blend compositions.

different crystalline modification in the PA6 and PA6/EBA blends. Generally in semicrystalline nylon-6 polymer there are two basic forms, α and γ.[42] The nylon-6 molecules are not centrosymmetric and are characterized by directionality to the molecule (NH—CO or CO—NH) such that if a molecule is imagined turned end-for-end it cannot be superimposed upon itself (Fig. 13[43]). The hydrogen-bonded sheets of α-phase of nylon-6 involve adjacent molecules which have opposite directionality and are

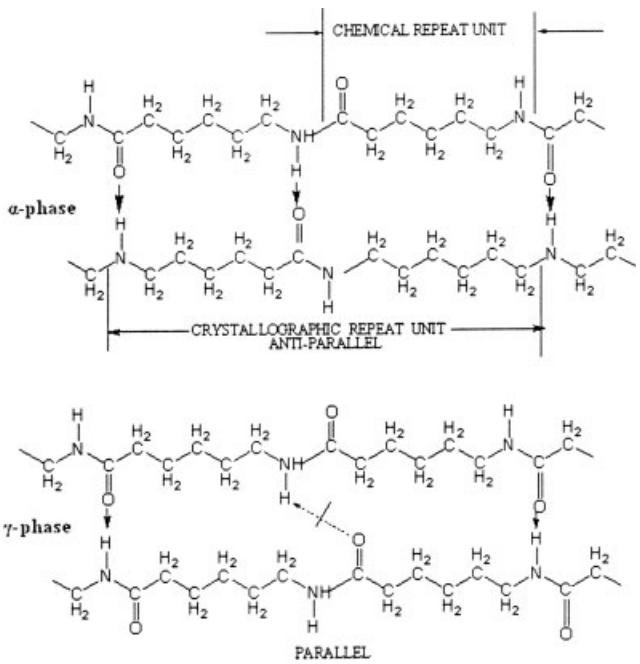

Figure 13 Schematic representation of nylon-6 macromolecule in α-phase and γ-phase crystallites.

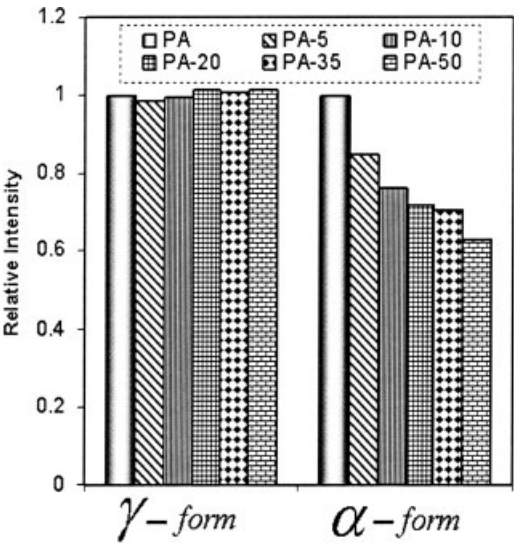

Figure 14 Variation of proportion of α-form and γ-form of nylon crystallites in various blend compositions.

said to be antiparallel. Arranged in this manner, all the hydrogen bond can be formed without strain. The α-form is characterized by the monoclinic unit cell with a zig–zag planar configuration, which has two repeat distances of 0.44 and 0.37 nm. Correspondingly, the peak reflection occurs at $2\theta = 20.5^\circ$ and 24°. If the adjacent molecules were of the same direction (parallel), only half of the hydrogen bonds could be formed. The hydrogen bonds are staggered up and down instead of always being displaced in the same direction. The γ-form consists of parallel chains with amide groups twisted from methylene group planes, where the repeat distance is 0.42 nm and the peak reflection 2θ angle is about 21.5°. In this study the pure nylon-6 exhibits two major crystalline modifications at $\sim 2\theta = 21.5^\circ$ and 24° (Fig. 12). This reveals that PA6 has crystallized in γ and α-form. It is worth noticing that due to the addition of EBA into nylon there is a change in the proportion of γ and α-form present in the system. Although the relative intensity of γ-form of crystals increases by 2% in the blends when compared to pure nylon-6, the relative intensity of α-form decreases drastically from 15 to 40% from PA-5 to PA-50 blends (Fig. 14). The increase in content of EBA decreases the proportion of α-form and slightly increases γ-form compared to pure nylon. This may be due to the possibility of mechanical restraints induced by the presence of EBA molecules, which favor the growth of γ-crystals and hinder the growth of α-crystals in PA6/EBA blends.

CONCLUSIONS

Nonisothermal crystallization kinetics studies of PA6 and PA6/EBA blends using various macrokinetic models such as Avrami and Jeziorny, Ozawa, Liu, Tobin, and Ziabicki provided a satisfactory description about the overall crystallization behavior of nylon-6 in the presence of varying proportion of EBA and in the absence of EBA. The predictions by Avrami reveal that the rate of the transformation is never constant during the nonisothermal process and rather increases with the time. The Avrami and Tobin parameter, n and n_t greater than 4 for pure nylon and PA6/EBA blends, suggest that all forms of the crystal growth such as fibrillar, disc-like, and spherulitic proceed at an increasing nucleation rate during nonisothermal crystallization. In the PA6/EBA blends, the finer and stable dispersion of EBA domains in the blends has decreased the crystallization rate when compared to pure EBA, especially at higher cooling rates in the primary crystallization stage, whereas it remained almost constant during secondary crystallization stage. Whereas during isothermal crystallization, crystallization process is mainly diffusion-controlled. The crystallization rate constant k values are higher for pure PA6 and PA-50. For pure PA6, the crystallization process was predominantly homogeneous, and in the absence of EBA domains, the nylon macromolecules were freely able to diffuse at a higher rate favoring faster growth of the crystals. Similarly at higher EBA content (PA-50), diffusion of nylon chains were unaffected by the presence of EBA domains, resulting in faster growth of crystals. However, in compositions such as PA-5, PA-10, PA-20, and PA-35, the tendency of gross phase separation and the rejection of EBA domains by growing crystal fronts, slightly lowered the chain mobility resulting in lesser values of k. Although Ozawa model fails to predict the nonisothermal crystallization behavior, combined Ozawa and Avrami model (Liu) provided a satisfactory description of the process. The values of $F(T)$ systematically increase with increasing relative degree of crystallinity, indicating that, at unit crystallization time, a higher cooling rate should be used to obtain a higher degree of crystallinity for all the compositions studied. Kinetic crystallizability G_{avg} calculated by Ziabicki method is to characterize the crystallizing ability of the polymer blend samples and was found to be in the order: PA-5 ≈ PA-50 > PA-10 ≈ PA > PA-35 > PA-20. The nucleation ability estimated by Dobreva and Gutzowa method indicates that EBA does not act as nucleating agent for the matrix nylon at lower concentration of EBA, whereas for EBA at higher concentration, it favored only the growth of γ-crystalline phase in nylon-6. The activation energies for the samples obtained from the Augis and Bennett, Kissinger, and Takhor were in the range of 288.73–249.91, 245.77–207.94, and 281.02–242.22 J/mol/K, respectively. The activation energy values were lower for the PA6/EBA blends because of

reduction in the proportion of α-crystalline phase when compared to pure PA6.

References

1. Sperling, L. H. Introduction to Physical Polymer Science, 2nd ed.; Wiley-Interscience: New York, 1992.
2. Chen, M.; Higg, P. G. J Chem Phys 1998, 108, 430.
3. Shanks, R. A.; Yu, L. Polymer Material Encyclopedia; CRC Press: Boca Raton, FL, 1996.
4. Yang, J.; McCoy, B. J.; Madras, G. J Chem Phys. 2005, 122, 064901.
5. Wunderlich, B. Macromolecular Physics. Crystal Structure, Morphology, Defects, Vol. 1.; Academic Press: New York, 1973.
6. Doye, J. K.; Frenkel, D. J Chem Phys 1998, 109, 10033.
7. Martuscelli, E. Polym Eng Sci 1984, 24, 563.
8. Araujo, E. M.; Hage, E.; Carvalho, A. J. F. J Mater Sci 2004, 39, 1173.
9. Lievana, E.; Karger-Kocsis, J. Macromol Symp 2003, 202, 59.
10. Chiou, K. C.; Wu, S. C.; Wu, H. D.; Chang, F. C. J Appl Polym Sci 1999, 74, 23.
11. Burgisi, G.; Paternoster, M.; Peduto, N.; Saraceno, A. J Appl Polym Sci 1997, 66, 777.
12. Ding, X. J.; Xu, R. W.; Yu, D. S.; Chen, H.; Fan, R. J Appl Polym Sci 2003, 90, 3503.
13. Balamurugan, G. P.; Maiti, S. N. Eur Polym J 2007, 43, 1786.
14. Lamberti, G. Heat Mass Transfer 2004, 41, 23.
15. Magill, H. Polymer 1961, 2, 221.
16. Turska, E.; Gogolewski, S. Polymer 1971, 12, 616.
17. Turska, E.; Goglewski S. J Appl Polym Sci 1975, 19, 637.
18. Avrami, M. J Chem Phys 1939, 7, 1103.
19. Avrami, M. J Chem Phys 1940, 8, 212.
20. Pan, B.; Yue, Q.; Ren, J.; Wang, H.; Jian, L.; Zhang, J.; Yang S. J Macomol Sci Part B Phys 2006, 45, 1025.
21. Christian, J. W. The Theory of Transformation in Metals and Alloys, 2nd ed.; Pergamon, Oxford, 1975.
22. Bartczak, Z.; Galeski, A.; Martuscelli, E. Polym Eng Sci 1984, 24, 1155.
23. Jeziorny, A. Polymer 1978, 19, 1142.
24. Weng, W.; Chen, G.; Wu, D. Polymer 2003, 44, 8119.
25. Ozawa, T. Polymer 1971, 12, 150.
26. Evans, U. R. Trans Faraday Soc 1945, 41, 365.
27. Liu, T.; Mo, Z.; Wang, S.; Zhang, H. Polym Eng Sci 1997, 37, 568.
28. Xu, J.; Feng, L.; Liu, Z.; Chen, L.; Deng, Y.; Cui, C.; Chen W. J Appl Polym Sci 1999, 71, 897.
29. Ziabicki, A. Appl Polym Symp 1967, 6, 1.
30. Ziabicki, A. Polymetry 1967, 12, 405.
31. Ziabicki, A. In Fundamentals of Fiber Spinning; Wiley: New York, 1976; pp 112–114.
32. Tobin, M. C. J Polym Sci Polym Phys 1974, 12, 399.
33. Tobin, M. C. J Polym Sci Polym Phys 1976, 14, 2253.
34. Tobin, M. C. J Polym Sci Polym Phys 1977, 15, 2269.
35. Dobreva, A.; Gutzow I. J Non-Cryst Solids 1993, 162, 1.
36. Dobreva, A.; Gutzow I. J Non-Cryst Solids 1993, 162, 13.
37. Augis, J. A.; Bennett, J. E. J Therm Anal 1978, 13, 283.
38. Kissinger, H. E. J Res Nat Bur Stand 1956, 57, 217.
39. Takhor, R. L. Advances in Nucleation and Crystallization of Glasses; American Ceramics Society: Columbus, 1971; pp 166–172.
40. Bosewell, P. G. J Therm Anal 1980, 18, 353.
41. Cascone, E.; Martuscelli, E.; Raimo, M. J Mater Sci 2001, 36, 3591.
42. Russell, D. P.; Beaumont, P. W. R. J Mater Sci 1980, 15, 197.
43. Melvin, I. K. Nylon Plastics; Wile: New York, 1973; pp 277–278.